Transp Porous Med (2016) 115:311–326
DOI 10.1007/s11242-016-0755-2

Particle Methods for Heat Transfer in Fractured Media

Viktoria R. Gisladottir[1] · **Delphine Roubinet**[2] · **Daniel M. Tartakovsky**[1]

Received: 26 January 2016 / Accepted: 8 August 2016 / Published online: 16 August 2016

Abstract Quantitative understanding of heat transfer in fractured media is critical in a wide range of applications, including geothermal energy harvesting. Mathematical models of such systems must account for fluid flow and heat transfer in both complex fracture networks and the ambient rock matrix. Incorporation of individual fractures with millimeter-scale apertures into meter-scale computational domains on which continuum models are discretized would be computationally prohibitive even on modern supercomputers. By exploiting the similarities of the underlying mathematical structure of heat and mass transfer processes, we adopt a mesh-free time-domain particle-tracking method to model heat transfer in highly heterogeneous fractured media. The method is used to model heat extraction from geothermal reservoirs whose fracture networks exhibit fractal properties representative of faults and damage zones. We explore a range of fracture network properties and experimental conditions in order to study the impact of the fracture network topology and hydraulic regimes on heat transfer. Our results demonstrate anomalous behavior of heat transfer in fractured environments and a significant impact of the network topology on performance of geothermal reservoirs.

Keywords Heat transfer · Fractured reservoir · Particle-tracking method · Anomalous transport · Geothermal performance

1 Introduction

Mathematical modeling of heat transfer in subsurface environments plays an important role in many fields of science and engineering. It has been used to optimize the performance of enhanced oil recovery by reducing oil viscosity with the injection of hot water or steam

✉ Daniel M. Tartakovsky
dmt@ucsd.edu

[1] Department of Mechanical and Aerospace Engineering, University of California, San Diego, 9500 Gilman Drive, MC 0411, La Jolla, CA 92093, USA

[2] Applied and Environmental Geophysics Group, Institute of Earth Sciences, University of Lausanne, Lausanne, Switzerland

(Al-Hadhrami and Blunt 2001) and ground heat exchangers used in cooling/heating of buildings (Ciriello et al. 2015), and to characterize subsurface environments by treating geothermal (Saar 2011) and anthropogenically generated (Wagner et al. 2014) heat as a groundwater tracer. It has also been deployed to forecast the adverse affects of subsurface heat generation and transfer, such as creation and/or reopening of microfractures leading to seismic activity induced by geothermal energy extraction (Chen and Shearer 2011) and nuclear waste leakage due to heat generated by radioactive decay (Wang et al. 1981).

In geothermal reservoirs, advection is the dominant mechanism of heat transfer within a fracture network, while the ambient matrix acts as the principal heat storage medium (Bruel 2002; Kolditz 1995; Ruiz Martinez et al. 2014). A network's topology determines the spatial extent of a heat extraction area, and the heat flux exchanged between fractures and the surrounding matrix controls the geothermal performance. The former can be modified with reservoir stimulation techniques (e.g., hydraulic fracturing), and the latter can be affected by varying hydraulic conditions (e.g., flow rates). Numerical models of heat transfer in fractured media facilitate design and implementation of both strategies.

These models must contend with a strong contrast in the hydraulic and thermal properties of fluid-filled fractures and the surrounding rock matrix, as well as with heterogeneous fracture networks that span a hierarchy of scales and often exhibit fractal behavior (Bonnet et al. 2001; de Dreuzy et al. 2001a, b). Such fractured media might not have a representative elementary volume. Hence, they are not amenable to standard homogenization (Long et al. 1982; Painter and Cvetkovic 2005; Roubinet et al 2010a) and modeling based on a single-continuum advection–dispersion equation (ADE). Two conceptual frameworks have been proposed to tackle this problem in the context of solute transport. The first treats a fractured rock as a stochastic continuum, whose transport properties are random fields; one postulates either the existence of a scale on which the (stochastic) ADE is valid (Neuman 2005) or the absence of such a scale by adopting instead, e.g., continuous-time random walk (CTRW) models (Berkowitz and Scher 1997). Both approaches predict anomalous (non-Fourier-like) average behavior of solute transport in fractured media (Scher et al. 2002; Neuman and Tartakovsky 2009; Cushman et al. 2011). CTRW has also been used to model the anomalous behavior of heat transfer in heterogenous and fractured media (Emmanuel and Berkowitz 2007; Geiger and Emmanuel 2010).

The second modeling framework explicitly incorporates dominant fractures into mathematical representations of the subsurface, i.e., replaces the continuum-medium representation of fractured rocks with two non-overlapping continua: a fluid-filled discrete fracture network (DFN) and the ambient rock matrix. Mass transfer models of this sort have been applied to both deterministic (Dverstorp et al. 1992; Nordqvist et al. 1992) and stochastic (Cacas et al. 1990; Ezzedine 2010) fracture networks. Numerical solutions of such models must combine a meter-scale discretization of the matrix with a millimeter-scale discretization of fracture apertures, which makes them computationally intensive, often prohibitively so. This has led to the development of mesh-free, particle-based solvers for solute transport in fractured rocks (Painter et al. 2008; Roubinet et al. 2010b). We are not aware of similar methods for heat transfer.

To study heat transfer due to injection of fluids into fractured geothermal reservoirs, we adopt the particle-based method of Roubinet et al. (2010b). The computational efficiency of this method allows us to handle site-specific fractal geometries of fracture networks characteristic of geothermal reservoirs and the hydraulic conditions representative of geothermal systems. Our simulations, conducted on a wide range of fracture network parameters and experimental conditions, reveal the anomalous behavior of heat transfer in heterogeneous fractured media. They also demonstrate the significant impact of the network properties

and hydraulic conditions on the performance of geothermal reservoirs. Section 2 contains a description of the fracture network and heat transfer models used in our analysis. In Sect. 3, we describe the mesh-free numerical method used to solve this problem and present a set of numerical experiments in Sect. 4. The simulation results are interpreted and discussed in Sect. 5.

2 Problem Formulation

To study geothermal energy harvesting, we consider fracture networks that are representative of geothermal reservoirs. The fracture network construction is described in Sect. 2.1, and models of fluid flow and heat transfer on these networks are formulated in Sects. 2.2 and 2.3, respectively.

2.1 Fracture Networks Models

Following Watanabe and Takahashi (1995), we consider a fractal fracture network model of geothermal reservoirs. The model defines the number of fractures N_f and the length r_i of the ith fracture ($i = 1, \ldots, N_\mathrm{f}$) as

$$N_\mathrm{f} = \mathtt{int}(C/r_0^D), \quad r_i = (C/i)^{1/D}, \tag{1}$$

where the function $\mathtt{int}(x)$ rounds x up to the next integer and D is the fractal dimension (a fitting parameter). The remaining two parameters, the fracture density C and the smallest fracture length r_0, can be estimated from a core sample. The fracture network is constructed by treating the midpoint of each fracture pair as a random variable. The angle between the pair of fractures can take one the two prescribed values, θ_1 or θ_2, with equal probability. The fracture's aperture b is constant and the same for all fractures.

2.2 Fluid Flow in the Network

We consider steady-state laminar flow of an incompressible fluid, which takes place in the fracture network while treating the ambient rock matrix as impervious. Assuming that a fracture is formed by two parallel smooth plates and that the fluid density ρ and dynamic viscosity μ remain constant, the Poiseuille law results in the average flow velocity u given by

$$u = -\frac{\rho g b^2}{12\mu} J. \tag{2}$$

Here, g is the gravitational acceleration constant, and J is the hydraulic head gradient along the fracture. Enforcing mass conservation at fracture junctions and applying expression (2) to each fracture segment leads to a linear system $\mathbf{Ah} = \mathbf{b}$ where $\mathbf{h}$ is the vector of the (unknown) hydraulic heads at fracture junctions (e.g., Long et al. 1982; de Dreuzy et al. 2001a). Given the global pressure gradient imposed on the outer edges of the network, we solve this linear system and use the resulting hydraulic heads to compute the average flow velocity in each fracture of the network.

2.3 Heat Transfer in Fracture–Matrix Systems

The particle method described in Sect. 3 constructs a solution to the problem of heat transfer in fracture networks from a solution to the problem of heat transfer in an individual fracture, with aperture b and semi-infinite length, embedded in an infinite matrix. The latter problem is formulated as follows. The fracture is represented by $\Omega_{\mathrm{f}} = \{(x, z) : 0 \leq x < \infty, |z| \leq b/2\}$ and the matrix by $\Omega_{\mathrm{m}} = \{(x, z) : 0 \leq x < \infty, |z| \geq b/2\}$. Fluid temperature in the fracture, $T^{\mathrm{f}}(x, z, t)$, satisfies an advection–dispersion equation (ADE)

$$\frac{\partial T^{\mathrm{f}}}{\partial t} + u\frac{\partial T^{f}}{\partial x} = D_L^{\mathrm{f}}\frac{\partial^2 T^{\mathrm{f}}}{\partial x^2} + D_T^{\mathrm{f}}\frac{\partial^2 T^{\mathrm{f}}}{\partial z^2}, \qquad (x, z) \in \Omega_{\mathrm{f}}, \tag{3}$$

where u is the fluid velocity computed in Sect. 2.2, and D_L^{f} and D_T^{f} are the longitudinal and transverse dispersion coefficients, respectively. These coefficients are defined as $D_L^{\mathrm{f}} = \lambda_L^{\mathrm{f}}/(\rho c) + E_L^{\mathrm{f}}/(\rho c)$ and $D_T^{\mathrm{f}} = \lambda_T^{\mathrm{f}}/(\rho c) + E_T^{\mathrm{f}}/(\rho c)$, where c is the fluid's heat capacity; λ_L^{f} and λ_T^{f} are the longitudinal and transverse thermal conductivity coefficients, respectively; and E_L^{f} and E_T^{f} are the longitudinal and transverse thermal dispersion coefficients, respectively (Yang and Yeh 2009).

Since the ambient matrix Ω_{m} is assumed to be impervious to flow, temperature in the matrix, $T^{\mathrm{m}}(x, z, t)$, is governed by a diffusion equation (DE)

$$\frac{\partial T^{\mathrm{m}}}{\partial t} = D_L^{\mathrm{m}}\frac{\partial^2 T^{\mathrm{m}}}{\partial x^2} + D_T^{\mathrm{m}}\frac{\partial^2 T^{\mathrm{m}}}{\partial z^2}, \quad (x, z) \in \Omega_{\mathrm{m}}, \tag{4}$$

where D_L^{m} and D_T^{m} are the longitudinal and transverse diffusion coefficients, respectively. These coefficients are defined as $D_L^{\mathrm{m}} = \lambda_L^{\mathrm{e}}/c_{\mathrm{e}}$ and $D_T^{\mathrm{m}} = \lambda_T^{\mathrm{e}}/c_{\mathrm{e}}$, where c_{e} is the effective heat capacity of the matrix, and λ_L^{e} and λ_T^{e} are the longitudinal and transverse thermal conductivity coefficients in the matrix, respectively.

At the fracture–matrix interfaces $|z| = b/2$, the continuity of both temperature and heat flux is enforced with conditions

$$T^{\mathrm{f}} = T^{\mathrm{m}}, \quad \phi_m D_T^{\mathrm{m}}\frac{\partial T^{\mathrm{m}}}{\partial z} = D_T^{\mathrm{f}}\frac{\partial T^{\mathrm{f}}}{\partial z}, \quad |z| = b/2, \tag{5}$$

where $\phi_m = [\phi + (1 - \phi)\rho_{\mathrm{s}}c_{\mathrm{s}}/(\rho c)]$; ϕ is the matrix porosity, and ρ_{s} and c_{s} are the density and heat capacity of the solid phase, respectively. Finally, Eqs. (3) and (4) are subject to initial conditions

$$T^{\mathrm{f}}(x, z, 0) = T_0, \quad T^{\mathrm{m}}(x, z, 0) = T_0, \tag{6}$$

and boundary conditions

$$T^{\mathrm{f}}(0, z, t) = T_{\mathrm{inj}}, \quad T^{\mathrm{f}}(+\infty, z, t) = T_0, \quad T^{\mathrm{m}}(x, \pm\infty, t) = T_0, \tag{7}$$

where $T_0(x, z)$ is the initial temperature in the system, and T_{inj} the temperature of the fluid injected at the entrance of the fracture.

Since the heat transfer problem (3)–(7) is invariant under transformations $T = T^i - T_0$ ($i = \mathrm{f}, \mathrm{m}$), we set, without loss of generality, $T_0 = 0$.

3 Particle Method for Heat Transfer in Fractured Media

Since the underlying mathematical structure of the heat and mass transfer problems is the same, we adapt the particle method of Roubinet et al. (2010b), which was developed to

model solute transport, to describe heat transfer in fractured rocks. The method consists of three parts: (i) at the fracture–matrix scale, heat transfer is described by advection in the fracture and conduction in the infinite matrix; (ii) at the matrix block scale, heat conduction in the matrix is restricted by the presence of neighboring fractures, into which particles can transfer; and (iii) at the fracture network scale, heat flux conservation is enforced at each fracture intersection by considering that the probability for a particle to enter a fracture depends on the intersection configuration and flow rate distribution.

At the fracture–matrix scale, we use the analytical solution of Tang et al. (1981), which is derived under the following simplifications of the boundary value problem (3)–(7). First, the ADE (3) is averaged over the fracture aperture to replace it with its one-dimensional counterpart. Second, longitudinal dispersion in the fracture is assumed to be negligible relative to convection. Third, diffusion in the matrix is assumed to be one-dimensional, in the direction perpendicular to the fracture. Finally, the flux continuity expressed by the second condition in (5) at the fracture–matrix interfaces is replaced by a source term in the fracture equation, which depends only on the matrix properties. Under these conditions, whose validity has been studied by Roubinet et al. (2012), the temperature distribution inside the fracture is given by

$$T^{\mathrm{f}}(x,t) = T_{\mathrm{inj}}\,\mathrm{erfc}\left(\frac{\phi_{\mathrm{m}}\sqrt{D_T^{\mathrm{m}}}x}{2ub\sqrt{t-x/u}}\right). \tag{8}$$

This expression is converted into a probabilistic model for a particle's diffusion time in infinite matrix, t_{d}^{∞}, as

$$t_{\mathrm{d}}^{\infty} = \left[\frac{\phi_m\sqrt{D_T^{\mathrm{m}}}t_{\mathrm{a}}}{2b\,\mathrm{erfc}^{-1}(R)}\right]^2, \quad t_a = \frac{x}{u} \tag{9}$$

where R is a uniform random number in the interval [0, 1], and t_{a} is the advection time spent in the fracture to reach the position x.

To take into account the impact of potential neighboring fractures (i.e., the finite size of matrix blocks), we consider the scenario of a fracture f_i surrounded by (i) a fracture f_1 located at distance l_1 on one side of f_i and (ii) a fracture f_2 located at distance l_2 on the other side of f_i. For each particle that diffuses into the matrix surrounding f_i, we define P^1_{transfer} as the probability to reach fracture f_1 without crossing fracture f_2 and P^2_{transfer} as the probability to reach fracture f_2 without crossing fracture f_1. These probabilities in the Laplace domain are given by (Feller 1954)

$$\tilde{P}^1_{\mathrm{transfer}} = \frac{\exp(l_1\sqrt{s/D_T^{\mathrm{m}}})}{s}\,\frac{1-\exp(-2l_2\sqrt{s/D_T^{\mathrm{m}}})}{1-\exp[2(l_1-l_2)\sqrt{s/D_T^{\mathrm{m}}}]} \tag{10a}$$

$$\tilde{P}^2_{\mathrm{transfer}} = \frac{\exp(l_2\sqrt{s/D_T^{\mathrm{m}}})}{s}\,\frac{1-\exp(-2l_1\sqrt{s/D_T^{\mathrm{m}}})}{1-\exp[2(l_2-l_1)\sqrt{s/D_T^{\mathrm{f}}}]}, \tag{10b}$$

where s is the Laplace variable. The numerical inversion of these expressions is performed with the Stehfest (1970) algorithm. The final diffusion time of each particle and its final position after diffusing in the matrix are computed in two steps. First, we determine P_{transfer}, the probability for a particle to transfer to one of the neighboring fractures with an associated transfer time t_{transfer} smaller than the maximum diffusion time t_{d}^{∞}, as

$$P_{\mathrm{transfer}} = P^1_{\mathrm{transfer}}\left(t_{\mathrm{transfer}} \le t_{\mathrm{d}}^{\infty}\right) + P^2_{\mathrm{transfer}}\left(t_{\mathrm{transfer}} \le t_{\mathrm{d}}^{\infty}\right). \tag{11}$$

Second, we pick a random number U from a uniform distribution on the interval [0, 1]: If U is larger than P_{transfer}, the particle does not transfer to the neighboring fractures (i.e., the particle goes back to its initial fracture) and its diffusion time is equal to t_{d}^{∞} (i.e., the assumption of infinite matrix is valid); otherwise, the particle transfers to one of the neighboring fractures, the transfer time is defined by solving $P_{\text{transfer}}(t \leq t_{\text{transfer}}) = U$, and the particle transfers to fracture f_1 if condition

$$\frac{U}{U_{\max}} > \frac{l_1}{l_1 + l_2} \tag{12}$$

is verified and to f_2 otherwise with $U_{\max} = P_{\text{transfer}}$. This method enables us to handle the presence of neighboring fractures in heterogeneous fracture networks. In the context of solute transport, a comparison between this approach and analytical solutions considering either a single fracture (Tang et al. 1981) or infinite systems of parallel fractures (Sudicky and Frind 1982) is provided in Roubinet et al. (2010b, 2013).

Finally, when a particle reaches a fracture intersection that forks into multiple fractures, both intersection configuration and flow rate distribution determine which fracture it enters. The particles can only enter into fractures that have a positive flow velocity (i.e., a fluid flowing from the studied intersection to another intersection) considering complete mixing and streamline routing rules (Hull and Koslow 1986; Berkowitz et al. 1994). In most cases, complete mixing is assumed and the probability for a particle to enter into a fracture is expressed as the ratio of the flow rate in the considered fracture to the sum of the flow rates leaving the studied intersection. A particular case is considered when a particle can enter two fractures: If the closest fracture has a dominant flow rate, the particle goes in priority to this fracture (Le Goc 2009).

4 Simulations of Heat Transfer in Geothermal Reservoirs

4.1 Geothermal Reservoir Properties

To study heat transfer in realistic geothermal reservoirs, we consider a square domain of length $L = 100$ m, whose left and right borders are connected by a fracture network. The latter has the fractal dimension $D = [1, 1.3]$ which has been observed in the natural environments (Main et al. 1990; Scholz et al. 1993), and fracture density $C = [2.5, 6.5]$ (Watanabe and Takahashi 1995). Three groups of fracture networks, *DFN1*, *DFN2* and *DFN3*, are defined with a fracture density set to $C = 2.5$, 4.5 and 6.5, respectively. For each group, we generate four fracture networks with a fractal dimension set to $D = 1$, 1.1, 1.2 and 1.3. Table 1 shows the parameters used to generate these fracture networks which are presented in Fig. 1.

Injection and extraction of fluid in these domains are simulated by considering injection and extraction wells located on the left and right borders of the domains, respectively. Two hydraulic regimes are applied between these wells in order to study different conditions of the geothermal exploitation. To this end, we define the *Fast Flows* regime where the head gradient is equal to 1.25 as considered in existing studies on geothermal systems (Suzuki et al. 2015). For comparison, we also define the *Slow Flows* regime where the head gradient is set to 10^{-2}. Considering a no-flow condition on the bottom and top borders of the domain, flow takes place from left to right through the interconnected fracture networks. The corresponding flow velocity fields are computed with the fluid density $\rho = 10^3$ kg/m^3 and the dynamic viscosity $\mu = 10^{-3}$ kg/(m s), on the interconnected fracture networks shown in Fig. 2.

Table 1 Parameters used to generate alternative fracture networks

	C [-]	D [-]	θ_1 [°]	θ_2 [°]	r_0 [m]	b [m]
DFN1a	2.5	1	25	145	10^{-1}	5×10^{-4}
DFN1b	2.5	1.1	25	145	10^{-1}	5×10^{-4}
DFN1c	2.5	1.2	25	145	10^{-1}	5×10^{-4}
DFN1d	2.5	1.3	25	145	10^{-1}	5×10^{-4}
DFN2a	4.5	1	25	145	10^{-1}	5×10^{-4}
DFN2b	4.5	1.1	25	145	10^{-1}	5×10^{-4}
DFN2c	4.5	1.2	25	145	10^{-1}	5×10^{-4}
DFN2d	4.5	1.3	25	145	10^{-1}	5×10^{-4}
DFN3a	6.5	1	25	145	10^{-1}	5×10^{-4}
DFN3b	6.5	1.1	25	145	10^{-1}	5×10^{-4}
DFN3c	6.5	1.2	25	145	10^{-1}	5×10^{-4}
DFN3d	6.5	1.3	25	145	10^{-1}	5×10^{-4}

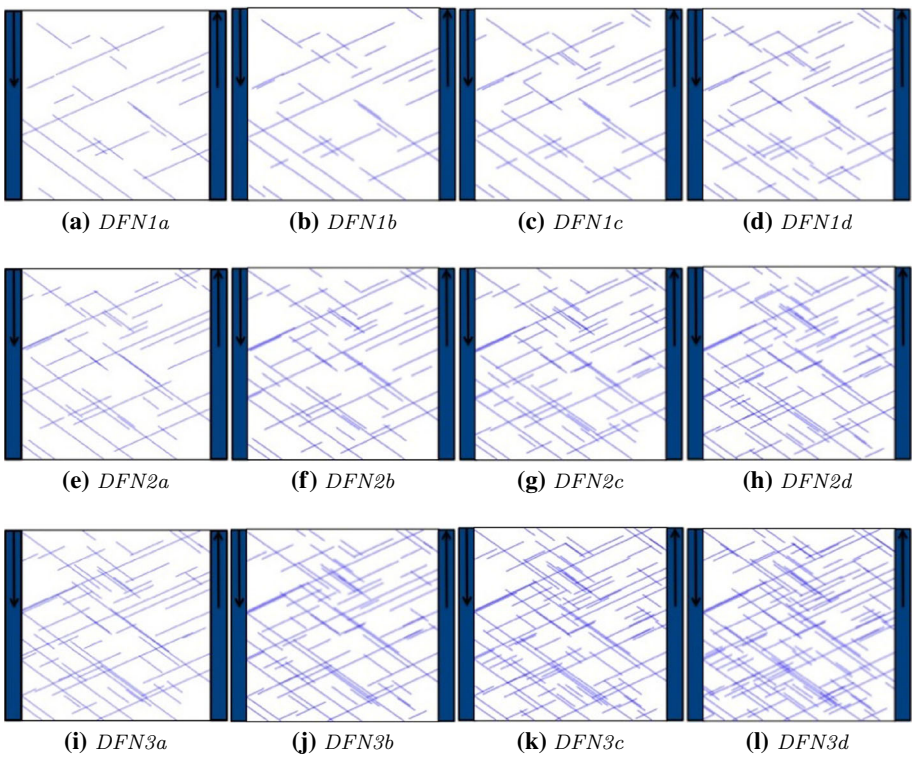

Fig. 1 Fracture networks generated with the fracture network parameters presented in Table 1. The *blue rectangles* on the *left* and *right* sides of the domains represent the injection and extraction wells of the geothermal systems, respectively

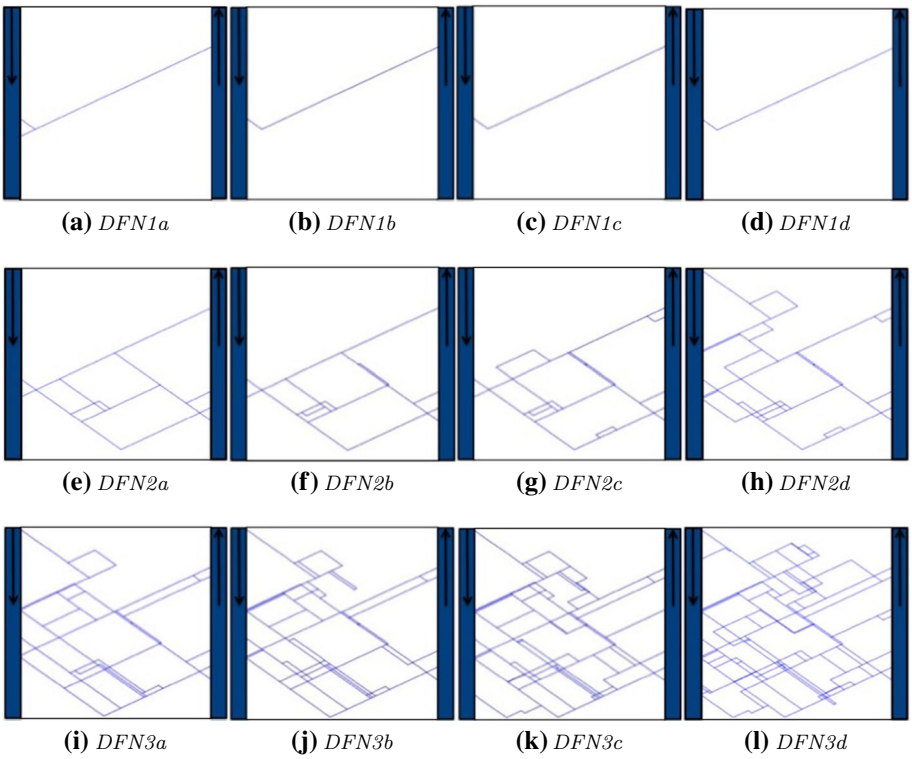

Fig. 2 Interconnected fracture networks related to the fracture networks presented in Fig. 1 and connecting the injection and extraction wells

4.2 Heat Transfer Simulations

Heat transfer is simulated in the interconnected fracture networks presented in Fig. 2 assuming an infinite matrix around each domain. For each fracture network and each flow regime, particles are injected into the fractures that intersect the injection well (left border of the domain), they are transported across the domain according to the heat transfer particle method presented in Sect. 3, and their arrival time to the production borehole (right border of the domain) is recorded. The rock porosity is $\phi = 0.1$ and the thermal parameters are provided in Table 2. These form data set (`i`) from Lippmann and Bödavarsson (1983), data set (`ii`) from Pruess et al. (1999), data set (`iii`) from Bödvarsson and Tsang (1982) and data set (`iv`) from Geiger and Emmanuel (2010).

Figure 3 exhibits the relative temperatures in the fracture network *DFN2a* with *Fast Flow* (Fig. 3a) and *Slow Flow* (Fig. 3b), for the thermal parameters representative of the values found in geothermal fields (Table 2). The between-set variability is not significant and has only minor impact on the temperature curves. Therefore, in the simulations presented below we use the parameter set (`ii`) in Table 2.

Figure 4 shows the corresponding relative temperature curves for the interconnected fracture networks *DFN1a*, *DFN2a* and *DFN3a* and the *Fast Flows* (Fig. 4a) and *Slow Flows* (Fig. 4b) regimes. In these figures, the relative temperature T^* is defined as

Table 2 Physical properties of fractured rocks used to simulate heat transfer

Parameter set	Values
(i)	
Thermal conductivity [W/(m °C)]	1.5
Rock density [kg/m^3]	2700
Rock heat capacity [J/(kg °C)]	920
(ii)	
Thermal conductivity [W/(m °C)]	2.1
Rock density [kg/m^3]	2650
Rock heat capacity [J/(kg °C)]	1000
(iii)	
Thermal conductivity [W/(m °C)]	2
Rock density [kg/m^3]	2500
Rock heat capacity [J/(kg °C)]	1000
(iv)	
Thermal conductivity [W/(m °C)]	2.5
Rock density [kg/m^3]	2500
Rock heat capacity [J/(kg °C)]	880

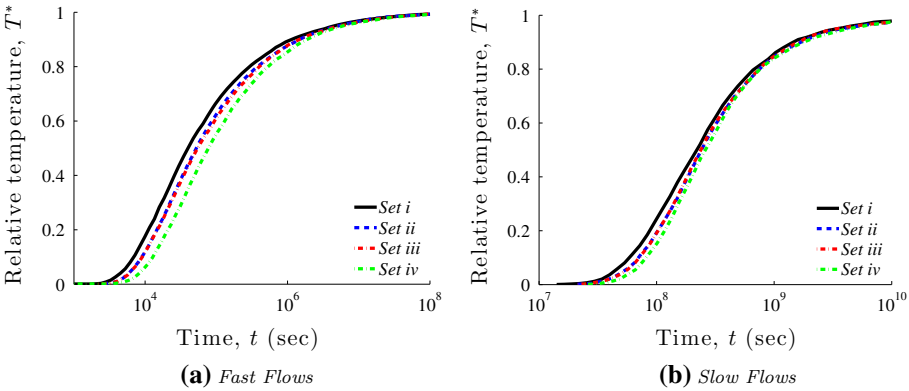

Fig. 3 Temporal variability of the relative temperature T^* in fracture network *DFN2a* with fractal dimension $D = 1$, for parameter sets (i)–(iv) in Table 2

$$T^* = \frac{T_{\text{ext}} - T_0}{T_{\text{inj}} - T_0} \tag{13}$$

where T_{ext} and T_{inj} are the fluid temperatures at extraction and continuous injection, respectively. These curves are obtained from the cumulative distribution functions (CDFs) of the particle arrival times using $N = 1855$ particles, and these results are similar to those obtained from 10^4 particles.

This empirical CDF $T^*(t)$ deviates significantly from the Gaussian CDF $\mathcal{G}(t)$, with the same mean $\bar{t}$ and standard deviation σ_t, over wide ranges of the fractal dimension D and fracture density C. This finding is reported in Table 3 in terms of the Kolmogorov–Smirnov

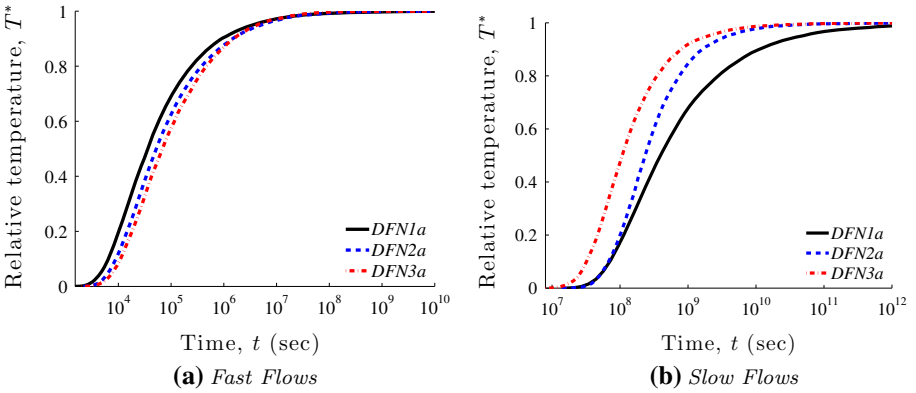

Fig. 4 Temporal variability of the relative temperature T^* in fracture networks *DFN1a*, *DFN2a* and *DFN3a* (see Fig. 2), for the matrix properties from data set `(ii)` in Table 2 and **a** *Fast Flows* and **b** *Slow Flows* conditions

Table 3 Kolmogorov–Smirnov statistic $\mathcal{S}_{\mathrm{KS}}$ for fracture networks characterized by their fractal dimension D and fracture density C

Fractal dimension, D	Fracture density, C	Kolmogorov–Smirnov statistic, $\mathcal{S}_{\mathrm{KS}}$
1.0	2.5	0.472
1.0	3.5	0.470
1.0	4.5	0.456
1.0	5.5	0.451
1.0	6.5	0.447
1.3	2.5	0.466
1.3	3.5	0.470
1.3	4.5	0.473
1.3	5.5	0.448
1.3	6.5	0.403

(KS) statistic (e.g., Lurie et al. 2011, Chapter 11.8)

$$\mathcal{S}_{\mathrm{KS}} \equiv \max_{1\le i\le N} |\mathcal{G}(t_i) - T^*(t_i)| = \max_{1\le i\le N} \left\{ \left| \mathcal{G}(t_{i-1}) - \frac{i-1}{N} \right|, \left| \frac{i}{N} - \mathcal{G}(t_i) \right| \right\} \tag{14}$$

where $\{t_1, \ldots, t_N\}$ are the particle arrival times arranged in the ascending order. The KS goodness of the fit test rules out the hypothesis that the CDF $T^*(t)$ is Gaussian and, hence, that heat transfer in fractured rocks follows Fourier's law, with any degree of confidence. For example, the 5 % (or 20 %) level of significance requires $\mathcal{S}_{\mathrm{KS}}$ not to exceed the critical value $\mathcal{S}^{\star}_{\mathrm{KS}} \approx 1.36/\sqrt{N} = 0.0316$ (or $\approx 1.07/\sqrt{N} = 0.0248$) (Lurie et al. (2011), [Table T-13]), but the values of $\mathcal{S}_{\mathrm{KS}}$ in Table 3 are more than an order of magnitude larger than $\mathcal{S}^{\star}_{\mathrm{KS}}$. Even with the caveat that the mean $\bar{t}$ and variance σ_t^2 of the Gaussian CDF $\mathcal{G}(t)$ should ideally be determined from simulations of an effective model rather than N samples, the discrepancy between $\mathcal{S}_{\mathrm{KS}}$ and $\mathcal{S}^{\star}_{\mathrm{KS}}$ is so large as to demonstrate the anomalous (non-Fourier-like) nature of heat transfer in fractured rocks.

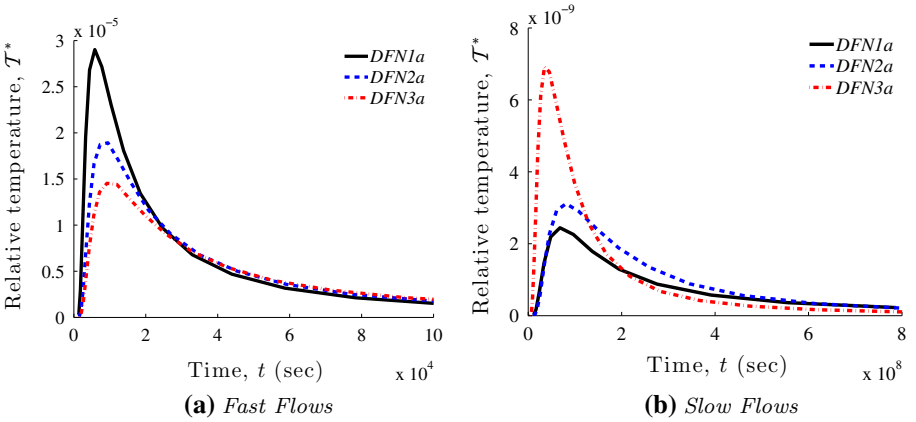

Fig. 5 Temporal variability of the relative temperature $\mathcal{T}^*$ in fracture networks *DFN1a*, *DFN2a* and *DFN3a* (see Fig. 2), for the matrix properties from data set (ii) in Table 2 and **a** *Fast Flows* and **b** *Slow Flows* conditions

To elucidate this anomalous behavior further, we define a relative temperature $\mathcal{T}^*$, which corresponds to the relative temperature T^* for an instantaneous temperature change of the injected fluid. Figure 5 shows the temperature distribution in the interconnected fracture networks *DFN1a*, *DFN2a* and *DFN3a* for the *Fast Flows* (Fig. 5a) and *Slow Flows* (Fig. 5b) hydraulic configurations. These results are obtained by transforming the CDFs presented in Fig. 4 into the probability density functions (PDFs). Here, 10^6 particles have been used in order to obtain smooth curves, and these results are similar to those obtained with 10^7 particles.

Geothermal performance of fractured reservoirs is often reported in terms of $P_\mathrm{f} = 1 - T^*$, such that $P_\mathrm{f} = 0$ represents the minimum efficiency of the system as the temperature of the extracted fluid is equal to the temperature of the (here cooler) injected fluid. Conversely, $P_\mathrm{f} = 1$ represents the maximum efficiency of the system as the temperature of the extracted fluid is equal to the (here warmer) initial temperature of the system. Figure 6 shows the temporal profiles $P_\mathrm{f}(t)$ for all considered fracture networks and for both the *Fast Flows* and *Slow Flows* hydraulic regimes. As in Fig. 4, these results are obtained using 10^3 particles and they are similar to those obtained from 10^4 particles.

5 Results and Discussion

5.1 Anomalous Heat Transfer

The results presented in Fig. 4 show a different behavior of T^* depending on the considered fracture density and flow regime. When T^* increases from 0 to 1, the temperature of the extracted fluid varies from the initial temperature in the system to the temperature of the injected fluid. This shows the progressive impact of the cooled injected fluid on the temperature of the extracted fluid due to the propagation of the cold front from the injection to the extraction wells. For *Fast Flows* (Fig. 4a), increasing the fracture density from *DFN1a* to *DFN3a* results in delaying the variations of T^*, showing that the cold front reaches the extraction well at longer times when considering larger fracture densities. In this case, the

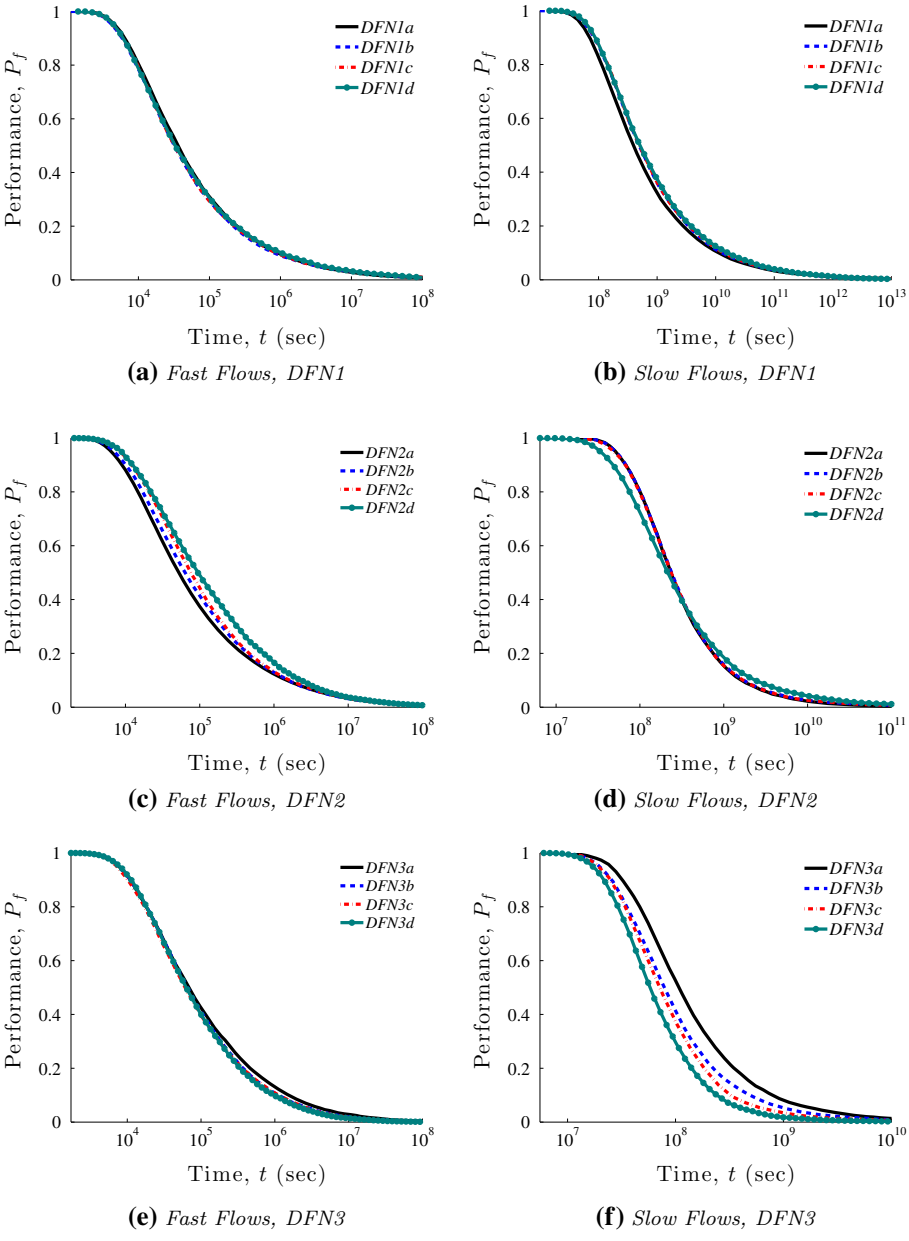

(a) *Fast Flows, DFN1* **(b)** *Slow Flows, DFN1*

(c) *Fast Flows, DFN2* **(d)** *Slow Flows, DFN2*

(e) *Fast Flows, DFN3* **(f)** *Slow Flows, DFN3*

Fig. 6 Temporal variability of the geothermal performance P_f of the fracture networks presented in Fig. 2 with the matrix properties from data set `(ii)` in Table 2, for the *Fast Flows* (left column) and *Slow Flows* (right column) conditions

complexity and density of the fracture networks determine the propagation of the cold front across the domain and increasing the fracture network density implies an increase in the time required to propagate from the left to right sides of the domain. Conversely, for *Slow Flows* (Fig. 4b), the impact of the cold front on the production well is delayed when the fracture

density decreases. In this case, the properties of the matrix blocks have a more important impact on the cold front propagation than the fracture network properties. For a small fracture densities (*DFN1a*), the cold front can propagate far away in the matrix without reaching a fracture, implying that this front reaches the extraction well at very large times. Increasing the fracture density (*DFN2a* and *DFN3a*) implies that the cold front propagation inside the matrix is limited by the presence of fractures, which results in reaching the exploitation well at smaller times. These results show that the impact of the geological structures on the propagation of a cold front depends on the hydraulic regime, as these structures determine if heat transfer is controlled by the fracture network properties or the size of the matrix blocks.

Converting the previous results into PDFs enables us to study the anomalous behavior of heat transfer in our simulations. As demonstrated by the heavy tails observed in Fig. 5, this anomalous behavior occurs for both *Fast Flows* (Fig. 5a) and *Slow Flows* (Fig. 5b) configurations. This is mostly due to the contrast between the fracture and matrix properties, as these structures are responsible for fast and slow heat propagation across the domain, respectively. However, the results presented in Fig. 4 reveal that this anomalous behavior is also related to the heterogeneities of each structure (fracture networks and matrix blocks) whose importance is determined by the hydraulic conditions. For *Fast Flows*, the fracture network complexity impacts the observed anomalous behavior. In this case, there is no impact of the matrix block heterogeneities as heat conduction inside these blocks is not limited by their size. Conversely, for *Slow Flows*, the matrix block size distribution impacts the observed anomalous behavior as heat conduction is limited by the size of these blocks.

5.2 Performance of Geothermal Systems

Figure 6 depicts the impact of both fracture density and fractal dimension on the performance of geothermal systems. The fracture networks with small fracture densities are not sensitive to the fractal dimension for both *Fast Flows* (Fig. 6a) and *Slow Flows* (Fig. 6b) conditions. This is due to the corresponding interconnected fracture networks which present small differences when changing the fractal dimension from 1 (Fig. 2a) to 1.1 (Fig. 2b) and no differences from 1.1 to 1.2 (Fig. 2c) and 1.3 (Fig. 2d). This shows the limitation of characterizing geothermal reservoirs only from core sampling as the related data do not give information on the connectivity of the domain. In terms of geothermal performance, this implies that reservoirs with different fracture network properties might have a nearly identical performance.

As the fracture density increases, from *DFN1* to *DFN3*, the impact of the fractal dimension D on the geothermal performance P_f depends on the hydraulic regime. For *Fast Flows* conditions (Fig. 6, left column), D does not have a significant impact on P_f, which is equal to 0 for times larger than 10^8 s. For *Slow Flows* conditions (Fig. 6, right column), D has a significant impact for the largest fracture density considered in this study (*DFN3*, Fig. 6f): An increase in the fractal dimension, from *DFN3a* to *DFN3d*, decreases the reservoir's performance. For *Slow Flows*, $P_\mathrm{f} = 0$ for times larger than 10^{12}, 10^{11} and 10^{10} s for the fracture networks *DFN1* (Fig. 6b), *DFN2* (Fig. 6d), and *DFN3* (Fig. 6f), respectively. This shows that increasing the fracture density causes the performance to decrease.

The different behavior of P_f for *Fast Flows* and *Slow Flows* conditions is related to the structural heterogeneities that control heat transfer in fractured domains. As demonstrated in Sect. 5.1, the fracture network and matrix block heterogeneities are determinant for *Fast Flows* and *Slow Flows* conditions, respectively, and, as demonstrated in Fig. 2, increasing the fracture density and fractal dimension results in more complex structures with more important heterogeneities. Therefore, broader distributions of the matrix block size are observed with the

presence of small blocks that limit heat conduction in the matrix and reduce the performance of the systems.

6 Conclusion

Quantitative understanding of heat transfer in heterogeneous fractured media is necessary for economically feasible harvesting of geothermal energy. We used a mesh-free particle-tracking method to model heat transfer in fractured geothermal reservoirs. This approach is capable of handling realistic discrete fracture networks and has computational efficiency that significantly exceeds that of standard (mesh-based) numerical methods. This enables us to conduct a series of two-dimensional heat transfer simulations for a large range of fracture network properties and experimental conditions and to interpret the corresponding results in terms of anomalous heat transfer and geothermal performance of reservoirs.

Our analysis leads to the following major conclusions.

1. Depending on hydraulic conditions, the propagation of a cold front across fractured domains is controlled by either the fracture network (*Fast Flows*) or matrix block (*Slow Flows*) properties.
2. The contrast of properties between fractures and matrix results in anomalous (non-Fourier-like) behavior of heat transfer, which is enhanced by heterogeneity of the fracture networks (*Fast Flows*) and matrix blocks (*Slow Flows*).
3. For small fracture densities ($C = 2.5$), different values of the fractal dimension ($D = [1, 1.3]$) can lead to identical interconnected fracture networks with similar geothermal performance.
4. In fractured domains with large fracture density ($C = 6.5$) and fractal dimension ($D = 1.3$), a broad distribution of the matrix block size is obtained with the presence of small blocks that reduce the geothermal performances under *Slow Flows* conditions.
5. Over a wide range of fracture densities and fractal dimensions, the heat transfer significantly deviates from the Fourier law, giving rise to anomalous effective behavior characterized by long tails.

Although the low computational cost of our method is attractive, some improvements could be introduced in future studies. These include incorporation of heterogeneity of matrix properties, implementation of two-dimensional convection by means of the analytical solutions developed by Ruiz Martinez et al. (2014) and extensions to three-dimensional conditions.

In the latter case, the modeled fractures will be represented as two-dimensional elements and the impact of the domain and structure dimensionality could be studied by progressively improving our model. For example, representing the fractures as rectangles with a one-dimensional flow (e.g., Lee et al. 2001) will allow us to evaluate the impact of the fracture network dimensionality. In comparison with two-dimensional simulations, the larger number of advective paths connecting the domain borders in three dimensions should lead to a larger distribution of the advection times spent in the fractures. These fractures could also be represented as ellipses (e.g., de Dreuzy et al. 2013) in which the heterogeneous flow velocity fields expand the distribution of advective times in comparison with the one-dimensional flow representation. As flow velocity in the fractures impacts heat propagation in both fractures and matrix, we also expect broader distributions of temperature of the extracted fluid with a significant anomalous behavior.

Finally, this study could be extended to more complex configurations where, for example, the impact of heterogeneous fracture apertures and randomly distributed fracture angles could

be considered. In order to evaluate the interest of representing different levels of heterogeneity, our work is related to the uncertainty in site characterization (de Barros et al. 2012; Ezzedine 2010) with Monte Carlo simulations.

Acknowledgments This work was supported in part by the National Science Foundation under Grant DMS-1522799. VRG was partially funded by a research scholarship from the DoD-SMART scholarship program.

References

Al-Hadhrami, H.S., Blunt, M.J.: Thermally induced wettability alteration to improve oil recovery in fractured reservoirs. SPE Reserv. Eval. Eng. **4**(3), 179–186 (2001)

Berkowitz, B., Scher, H.: Anomalous transport in random fracture networks. Phys. Rev. Lett. **79**(20), 4038 (1997)

Berkowitz, B., Naumann, C., Smith, L.: Mass transfer at fracture intersections: an evaluation of mixing models. Water Resour. Res. **30**(6), 1765–1773 (1994)

Bödvarsson, G.S., Tsang, C.F.: Injection and thermal breakthrough in fractured geothermal reservoirs. J. Geophys. Res. Solid Earth **87**(B2), 1031–1048 (1982)

Bonnet, E., Bour, O., Odling, N.E., Davy, P., Main, I., Cowie, P., Berkowitz, B.: Scaling of fracture systems in geological media. Rev. Geophys. **39**(3), 347–383 (2001)

Bruel, D.: Impact of induced thermal stresses during circulation tests in an engineered fractured geothermal reservoir—example of the Soultz-sous-Forets European Hot Fractured Rock Geothermal Project, Rhine Graben, France. Oil Gas Sci. Technol. Rev. IFP **57**(5), 459–470 (2002)

Cacas, M.C., Ledoux, E., de Marsily, G., Barbreau, A., Calmels, P., Gaillard, B., Margritta, R.: Modeling fracture flow with a stochastic discrete fracture network: calibration and validation: 2. The transport model. Water Resour. Res. **26**(3), 491–500 (1990)

Chen, X., Shearer, P.M.: Comprehensive analysis of earthquake source spectra and swarms in the Salton Trough, California. J. Geophys. Res. Solid Earth **116**(B09), 309 (2011)

Ciriello, V., Bottarelli, M., Di Federico, V., Tartakovsky, D.M.: Temperature fields induced by geothermal devices. Energy **93**(2), 1896–1903 (2015)

Cushman, J.H., Park, M., Moroni, M., Kleinfelter-Domelle, N., O'Malley, D.: A universal field equation for dispersive processes in heterogeneous media. Stoch. Environ. Res. Risk Assess. **25**(1), 1–10 (2011)

de Barros, F.P.J., Ezzedine, S., Rubin, Y.: Impact of hydrogeological data on measures of uncertainty, site characterization and environmental performance metrics. Adv. Water Resour. **36**, 51–63 (2012)

de Dreuzy, J.R., Davy, P., Bour, O.: Hydraulic properties of two-dimensional random fracture networks following a power law length distribution: 1. Effective connectivity. Water Resour. Res. **37**(8), 2065–2078 (2001a)

de Dreuzy, J.R., Davy, P., Bour, O.: Hydraulic properties of two-dimensional random fracture networks following a power law length distribution: 2. Permeability of networks based on lognormal distribution of apertures. Water Resour. Res. **37**(8), 2079–2095 (2001b)

de Dreuzy, J.R., Pichot, G., Poirriez, B., Erhel, J.: Synthetic benchmark for modeling flow in 3D fractured media. Comput. Geosci. **50**, 59–71 (2013)

Dverstorp, B., Andersson, J., Nordqvist, W.: Discrete fracture network interpretation of field tracer migration in sparsely fractured rock. Water Resour. Res. **28**(9), 2327–2343 (1992)

Emmanuel, S., Berkowitz, B.: Continuous time random walks and heat transfer in porous media. Transp. Porous Media **67**(3), 413–430 (2007)

Ezzedine, S.: Impact of geological characterization uncertainties on subsurface flow using stochastic discrete fracture network models. In: Annual Stanford Workshop on Geothermal Reservoir Engineering, Stanford, CA (2010)

Feller, W.: Diffusion processes in one dimension. Trans. Am. Math. Soc. **77**, 1–31 (1954)

Geiger, S., Emmanuel, S.: Non-Fourier thermal transport in fractured geological media. Water Resour. Res. **46**(7), W07504 (2010). doi:10.1029/2009WR008671

Hull, L.C., Koslow, K.N.: Streamline routing through fracture junctions. Water Resour. Res. **22**(12), 1731–1734 (1986)

Kolditz, O.: Modelling flow and heat transfer in fractured rocks: dimensional effect of matrix heat diffusion. Geothermics **24**(3), 421–437 (1995)

Le Goc, R.: Caractérisation et modélisation des écoulements dans les milieux fracturés. Thèse de doctorat, Université de Rennes 1 (2009)

Lee, S.H., Lough, M.F., Jensen, C.L.: Hierarchical modeling of flow in naturally fractured formations with multiple length scales. Water Resour. Res. **37**(3), 443–455 (2001)
Lippmann, M.J., Bödavarsson, G.S.: Numerical studies of the heat and mass transport in the Cerro Prieto geothermal field, Mexico. Water Resour. Res. **19**(3), 753–767 (1983)
Long, J.C.S., Remer, J.S., Wilson, C.R., Witherspoon, P.A.: Porous media equivalents for networks of discontinuous fractures. Water Resour. Res. **18**(3), 645–658 (1982)
Lurie, D., Abramson, L., Vail, J.: Applying statistics. Tech. Rep. NUREG/CR-1475, Rev 1, United States Nuclear Regulatory Comission, Washington, DC (2011)
Main, I.G., Meredith, P.G., Sammonds, P.R., Jones, C.: Influence of fractal flaw distributions on rock deformation in the brittle field. Geol. Soc. Lond. **54**(1), 81–96 (1990). (Special Publications)
Neuman, S.P.: Trends, prospects and challenges in quantifying flow and transport through fractured rocks. Hydrogeol. J. **13**(1), 124–147 (2005)
Neuman, S.P., Tartakovsky, D.M.: Perspective on theories of non-Fickian transport in heterogeneous media. Adv. Water Resour. **32**(5), 670–680 (2009)
Nordqvist, A.W., Tsang, Y.W., Tsang, C.F., Dverstorp, B., Andersson, J.: A variable aperture fracture network model for flow and transport in fractured rocks. Water Resour. Res. **28**(6), 1703–1713 (1992)
Painter, S., Cvetkovic, V.: Upscaling discrete fracture network simulations: an alternative to continuum transport models. Water Resour. Res. **41**, W02002 (2005). doi:10.1029/2004WR003682
Painter, S., Cvetkovic, V., Mancillas, J., Pensado, O.: Time domain particle tracking methods for simulating transport with retention and first-order transformation. Water Resour. Res. **44**, W01406 (2008). doi:10.1029/2007WR005944
Pruess, K., Oldenburg, C., Moridis, G.: TOUGH2 User's Guide Version 2. Lawrence Berkeley National Laboratory, Berkeley (1999)
Roubinet, D., de Dreuzy, J.R., Davy, P.: Connectivity-consistent mapping method for 2-D discrete fracture networks. Water Resour. Res. **46**(7), W07532 (2010a)
Roubinet, D., Liu, H.-H., de Dreuzy, J.-R.: A new particle-tracking approach to simulating transport in heterogeneous fractured porous media. Water Resour. Res. **46**(11), W11507 (2010b). doi:10.1029/2010WR009371
Roubinet, D., de Dreuzy, J.R., Tartakovsky, D.M.: Semi-analytical solutions for solute transport and exchange in fractured porous media. Water Resour. Res. **48**(1), W01,542 (2012)
Roubinet, D., de Dreuzy, J.R., Tartakovsky, D.M.: Particle-tracking simulations of anomalous transport in hierarchically fractured rocks. Comput. Geosci. **50**, 52–58 (2013)
Ruiz Martinez, A., Roubinet, D., Tartakovsky, D.M.: Analytical models of heat conduction in fractured rocks. J. Geophys. Res. Solid Earth **119**(1), 83–98 (2014)
Saar, M.: Review: Geothermal heat as a tracer of large-scale groundwater flow and as a means to determine permeability fields. Hydrogeol. J. **19**(1), 31–52 (2011)
Scher, H., Margolin, G., Berkowitz, B.: Towards a unified framework for anomalous transport in heterogeneous media. Chem. Phys. **284**(1–2), 349–359 (2002)
Scholz, C., Dawers, N., Yu, J.Z., Anders, M., Cowie, P.: Fault growth and fault scaling laws: preliminary results. J. Geophys. Res. Solid Earth **98**(B12), 21951–21961 (1993)
Stehfest, H.: Algorithm 368: numerical inversion of Laplace transform. Commun ACM **13**(1), 47–49 (1970)
Sudicky, E.A., Frind, E.O.: Contaminant transport in fractured porous media: analytical solutions for a system of parallel fractures. Water Resour. Res. **18**(6), 1634–1642 (1982)
Suzuki, A., Niibori, Y., Fomin, S.A., Chugunov, V.A., Hashida, T.: Analysis of water injection in fractured reservoirs using a fractional-derivative-based mass and heat transfer model. Math. Geosci. **47**(1), 31–49 (2015)
Tang, D.H., Frind, E.O., Sudicky, E.A.: Contaminant transport in fractured porous media: analytical solution for a single fracture. Water Resour. Res. **17**(3), 555–564 (1981)
Wagner, V., Li, T., Bayer, P., Leven, C., Dietrich, P., Blum, P.: Thermal tracer testing in a sedimentary aquifer: field experiment (Lauswiesen, Germany) and numerical simulation. Hydrogeol. J. **22**(1), 175–187 (2014)
Wang, J.S.Y., Tsang, C.F., Cook, N.G.W., Witherspoon, P.A.: A study of regional temperature and thermo-hydrologic effects of an underground repository for nuclear wastes in hard rock. J. Geophys. Res. Solid Earth **86**(B5), 3759–3770 (1981)
Watanabe, K., Takahashi, H.: Fractal geometry characterization of geothermal reservoir fracture networks. J. Geophys. Res. Solid Earth **100**(B1), 521–528 (1995)
Yang, S.Y., Yeh, H.D.: Modeling heat extraction from hot dry rock in a multi-well system. Appl. Therm. Eng. **29**(8–9), 1676–1681 (2009)